© 2015. Published by The Company of Biologists Ltd | Development (2015) 142, 1661-1671 doi:10.1242/dev.120287

RESEARCH ARTICLE

Clonal analysis reveals granule cell behaviors and compartmentalization that determine the folded morphology of the cerebellum

Emilie Legué[1,*], Elyn Riedel[2] and Alexandra L. Joyner[1,‡]

ABSTRACT

The mammalian cerebellum consists of folds of different sizes and shapes that house distinct neural circuits. A crucial factor underlying foliation is the generation of granule cells (gcs), the most numerous neuron type in the brain. We used clonal analysis to uncover global as well as folium size-specific cellular behaviors that underlie cerebellar morphogenesis. Unlike most neural precursors, gc precursors divide symmetrically, accounting for their massive expansion. We found that oriented cell divisions underlie an overall anteroposteriorly polarized growth of the cerebellum and gc clone geometry. Clone geometry is further refined by mediolateral oriented migration and passive dispersion of differentiating gcs. Most strikingly, the base of each fissure acts as a boundary for gc precursor dispersion, which we propose allows each folium to be regulated as a developmental unit. Indeed, the geometry and size of clones in long and short folia are distinct. Moreover, in engrailed 1/2 mutants with shorter folia, clone cell number and geometry are most similar to clones in short folia of wild-type mice. Thus, the cerebellum has a modular mode of development that allows the plane of cell division and number of divisions to be differentially regulated to ensure that the appropriate number of cells are partitioned into each folium.

KEY WORDS: Foliation, Lineage restriction, Lobules, Morphogenesis, Polarized growth, Engrailed mutants, Mouse

INTRODUCTION

In order to produce an organ with a specific shape, the correct number of cells of different lineages must be produced and precisely spatially arranged during development. Moreover, the proper spatial organization of cells in an organ is necessary for its function. In the brain, the cortex of the mammalian cerebellum (Cb) (Fig. 1A,B) and the neocortex (dorsal forebrain) of gyrencephalic mammals have a folded morphology that accommodates a large number of functionally diverse neural circuits. Each cerebellar fold receives a distinct combination of afferent inputs and therefore can be thought of as a functional unit (Larsell, 1952; Sillitoe and Joyner, 2007). Recent studies indicate that cells with one radial process projecting to the pial surface play a key role in producing folds. In the neocortex of gyrencephalic mammals, basal radial glial cells seem to be responsible for the formation of the folds, or gyri and sulci (Nonaka-Kinoshita et al., 2013; Stahl et al., 2013). In the cerebellar cortex of mice, the base of each fissure that separates two folds (folia) has a distinct cellular organization of Bergmann glial radial fibers and associated granule cell progenitors (gcps), referred to as anchoring centers (see Fig. 9) (Sudarov and Joyner, 2007). Moreover, the pattern of cerebellar folds is conserved between species, suggesting developmental regulation of the allocation of cells to each fold. Indeed, in mouse mutants lacking alleles of engrailed 1 and 2 (*En1/2*) homeobox genes, the timing and placement of particular anchoring centers in the Cb is altered and is accompanied by changes in the shape of the intervening folia (Cheng et al., 2010; Millen et al., 1994; Orvis et al., 2012; Sgaier et al., 2007). It is therefore crucial to understand how the correct number of cells is allocated to each folium to produce the foliation pattern essential for normal cerebellar circuit formation and function.

The generation of distinct organ shapes during development depends on local differences (anisotropies) in the behavior of cells (Kennaway et al., 2011), including different rates of cell division or differentiation, oriented cell growth or migration, non-random cell mixing and oriented intercalation. Non-random cell mixing can lead to the formation of boundaries that separate cells of the same lineage into different compartments that receive distinct developmental cues and thus produce diversity within an organ (Vincent, 1998). Clonal analysis is an ideal tool for revealing anisotropies in cell behaviors and developmental boundaries that underlie organ shape. As only the Cb of mice undergoes folding, and since granule cell (gc) production is crucial for foliation, we have applied a clonal analysis to the gcps of wild-type (WT) and *En1/2* mutant mice in order to identify cellular behaviors that account for the distinct shape and size of each folium.

An increase or decrease in the production of gcs results in a corresponding change in the size of folia (Altman et al., 1969; Bohn and Lauder, 1980; Corrales et al., 2006; Lewis et al., 2004; Noguchi et al., 2008). Gcs are generated by a unique germinal zone termed the external gc layer (EGL), which covers the surface of the mouse Cb from embryonic day (E) 15.5 to postnatal day (P) 16 (Altman and Bayer, 1997; Sillitoe and Joyner, 2007; Sudarov and Joyner, 2007). The gcps are produced by the upper rhombic lip, a structure located at the caudal end of the Cb primordium, and migrate over the surface of the Cb primordium to form the EGL (Fig. 1B,C). There is a temporal relationship between the time when the gcps exit the rhombic lip and their final anterior-posterior (AP) position in the EGL, with the gcps that exit first (E13.5) residing more anteriorly than those that exit later (Machold and Fishell, 2005). Accordingly, early clonal marking of chick gcps leaving the rhombic lip produced clones that spread mainly along the AP axis and spanned many folia (Ryder and Cepko, 1994). However, gcp behaviors that govern foliation after establishment of the EGL,

[1]Department of Developmental Biology, Memorial Sloan-Kettering Cancer Center, 1275 York Avenue, New York, NY 10065, USA. [2]Department of Epidemiology and Biostatistics, Memorial Sloan-Kettering Cancer Center, 1275 York Avenue, New York, NY 10065, USA.
*Present address: Yale University School of Medicine, Department of Pediatrics, 333 Cedar Street, New Haven, CT 06520, USA.

‡Author for correspondence (joynera@mskcc.org)

Received 24 November 2014; Accepted 9 March 2015

Development (2015) 142, 1661-1671 doi:10.1242/dev.120287

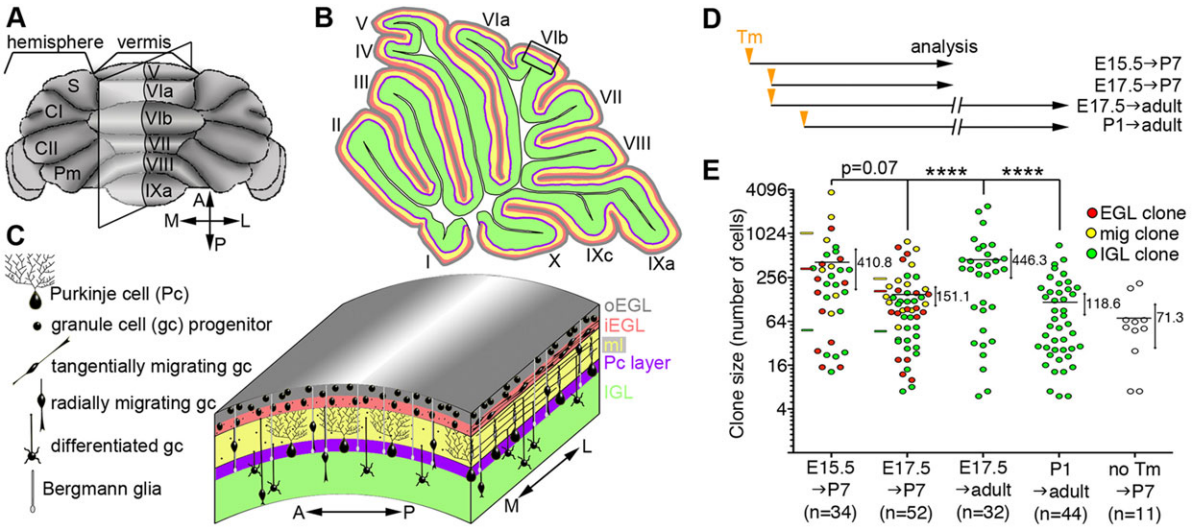

Fig. 1. The average size of gc clones correlates with the length of the growth phase. (A) Dorsal view of whole cerebellum (Cb). (B) Midsagittal section of Cb and (C) 3D representation of cerebellar cortex (boxed region in B) with layers and cell types indicated. (D) Experimental design indicating time of tamoxifen (Tm) injection and analysis of *Atoh1-CreER/+;R26R*$^{LSL\text{-}YFP/+}$ mice. (E) The number of cells in each clone in the different datasets is plotted on a $\log_2$ scale, with the mean size (black line all clones; colored lines for corresponding subtype) and 95% confidence interval (vertical double arrow) shown. ****P<0.0001 (P-values were calculated from linear regression models with generalized estimating equations). A, anterior; P, posterior; M, medial; L, lateral; S, simplex; Cl and II, Crus I and II; Pm, paramedian; oEGL, outer external granule cell layer; iEGL, inner external granule cell layer; ml, molecular layer; IGL, internal granule cell layer.

during the period of major cerebellar growth and fissure formation, remain to be elucidated.

The cells within a gcp clone have the unusual stem cell property of dividing only symmetrically in the outer layer of the EGL (oEGL) and then differentiating *en masse* over a 2-day period, at a time chosen seemingly randomly between E18.5 and P16.5 (Espinosa and Luo, 2008). Newly born gcs then go through an initial tangential migration along the medial-lateral (ML) axis in the inner part of the EGL (iEGL) (Komuro et al., 2001), a subsequent radial migration along the radial fibers of Bergmann glia, and a final migration in the internal gc layer (IGL) (Fig. 1C) (Chédotal, 2010; Komuro and Rakic, 1995, 1998). Interestingly, the parallel fibers of gcs stack in an inside to outside temporal manner forming a molecular layer (ml) above the IGL, whereas the cell bodies of clonally related gcs are randomly positioned in the IGL (Espinosa and Luo, 2008; Zong et al., 2005). It is not known, however, whether there is a polarization to gcp dispersion in the EGL and/or to the tangential migration of gcs that can account for the preferential growth of the Cb along the AP axis after birth, whether anchoring centers influence gcp dispersion (e.g. act as boundaries), or whether clone size and geometry relate to the diversity of folium shapes.

In order to discover cellular behaviors that underlie the shaping of cerebellar folia after the EGL is established, we evaluated the geometry of gc clones, their cell number and cell dispersion properties with respect to folium size and timing of marking. We found that dispersion of gcps within clones is significantly polarized along the AP axis and correlates with a preferential AP orientation of the plane of gcp division. During tangential migration, the initial ML length of clones is expanded. In the IGL, early born gcs have the greatest dispersion, owing to the intercalation of later born gcs. Most extraordinarily, the gcps within a clone do not cross through established anchoring centers. Moreover, the geometry and number of gcs in clones residing in short folia are significantly different from those in long folia. We propose that anchoring centers act to compartmentalize gcp clones, which allows for differential regulation of cellular behaviors in each folium and thus the generation of folia diversity. To test this hypothesis, we characterized gc clones in *En1*$^{-/+}$*;En2*$^{-/-}$ mice that have a diminished Cb (Sgaier et al., 2007) and indeed found that clones were smaller with a reduced AP polarization. Our study has uncovered a set of progenitor cell behaviors that underlie the shaping of the cerebellar folia, and could have implications for the stereotyped folding pattern of the human neocortex.

RESULTS

Exquisite synchronization of differentiation of clonally related gcps

Based on the knowledge that clones generated from single gcps at E17.5 form clusters restricted to discrete portions of one or two folia (Espinosa and Luo, 2008), we adapted the genetic inducible fate-mapping approach for gcp clonal analyses (Brownell et al., 2011; Legue et al., 2010) by combining an *Atoh1-CreER*^{T2} transgene (Machold and Fishell, 2005) and *R26R*$^{LSL\text{-}YFP}$ (Srinivas et al., 2001) reporter. We empirically determined the clonal dose of tamoxifen (Tm) as that producing <25 clones per Cb (supplementary material Table S1). In the absence of Tm, 1.8 clones were detected per mouse on average (supplementary material Table S1), and thus <13% of all the clones analyzed were spontaneous clones. Three developmental stages were chosen for marking: E15.5, before initiation of foliation; E17.5, when only a few fissures have formed; and P1, when most fissures have formed. Analysis of the clones was carried out at P7 to analyze all stages of gc development, and at P21 to P30 (adult). We generated four sets of clones: E15.5→P7, E17.5→P7, E17.5→adult and P1→adult (Fig. 1D; supplementary material Table S2).

In order to uncover gcp behaviors that determine Cb foliation, we first validated our approach by comparing the number of cells in E17.5→adult clones with the clones produced by the mosaic analysis using double markers (MADM) technique (Espinosa and Luo, 2008). Indeed, the two methods produced clones with similar average sizes [446.3 (Fig. 1E) and 480 (Espinosa and Luo, 2008) cells]. Furthermore, we found that gc clones differentiate *en masse* at P7 (Espinosa and Luo, 2008; Zong et al., 2005). Three subtypes of gcs are present at P7: proliferating gcps in the oEGL (EGL

Development (2015) 142, 1661-1671 doi:10.1242/dev.120287

subtype, supplementary material Fig. S1A), migrating gcs in the iEGL or ml (mig subtype, supplementary material Fig. S1B), and gcs in the IGL (IGL subtype, supplementary material Fig. S1C). As expected, less than 10% of the clones analyzed at P7 (E15.5→P7 or E17.5→P7 clones) contained all three gc subtypes, and most clones (~80%) contained either only one gc subtype or with one representing >75% of the cells (supplementary material Fig. S1D, Table S3). Thus, all clones had a high degree of subtype homogeneity. Given that it takes a gc ~40 h to move from the oEGL to the IGL (Komuro and Yacubova, 2003), a clone must become postmitotic and migrate to the IGL within a tight time window (Espinosa and Luo, 2008; Zong et al., 2005). We classified the P7 clones as EGL, migrating (mig) or IGL clones based on the gc subtype that dominated in the clone.

Clone cell number is proportional to the time spent in the EGL

A surprising conclusion of the MADM study based on the analysis of E17.5→adult gc clones was that the same range of clone sizes is generated whether clones differentiate early or late (Espinosa and Luo, 2008), based on the position of the parallel fibers of clones. In accordance with the MADM study, we found a wide range in the size of clones using each marking scheme (Fig. 1E). However, E17.5→P7 clones were significantly smaller than the E17.5→adult clones ($P<0.0001$). Similarly, adult clones were significantly larger when induced at E17.5 rather than at P1 ($P<0.0001$), and P7 clones were larger when marked at E15.5 rather than at E17.5 ($P=0.07$) (Fig. 1E). Using the position of parallel fibers in the ml (supplementary material Fig. S2A-C) as an indication of the timing of differentiation of clones, we also found a significant correlation between the length of growth and size of a clone (supplementary material Fig. S2D, Spearman rank correlation coefficient $r=0.83$, $P=0.003$). Thus, by directly determining the sizes of clones with different lengths of time to expand we found that, on average, clones with longer to grow have a greater number of cells.

Poor synchronization of cell cycle phase in clonally related gcps

Given that cells in a gcp clone become postmitotic over a short time period, we tested whether cells within a clone are synchronized with respect to the phase of the cell cycle. E17.5→P7 clones were administered the uridine analog EdU to mark cells undergoing the phase of DNA synthesis (S phase) (Fig. 2A) 30 min before harvesting the Cb. We reasoned that if the cells within a clone are synchronized in their cell cycle, then all cells within a clone should either be in S phase (EdU^+) or not (EdU^-), whereas if the cells within a clone are not synchronized then the S-phase index of the clone (percentage of cells in S phase) should resemble that of the surrounding oEGL cells.

As expected (Fujita, 1967), the S-phase index of the oEGL cells surrounding all the EGL clones analyzed ($n=18$, 412-5720 cells analyzed) was ~40%, with little variation (±4%) (Fig. 2B). Of the 18 EGL clones analyzed for EdU incorporation, seven contained a small percentage of cells (<10%) in the iEGL that had begun differentiating. Consistent with previous findings at P9 (Espinosa and Luo, 2008), such clones had a higher average S-phase index than pure oEGL clones (46.9% versus 34.6%) and a greater cell number (Fig. 2C,D), consistent with the proposal that gcps increase their proliferation rate during final rounds of cell division. Surprisingly, we found a high variation in the S-phase index of the pure oEGL clones ($n=11$; 9.1% to 64.1%, s.d.=15.2%, Fig. 2C,D), which could reflect that each clone has a different rate of proliferation or that there is a partial synchronization of the phase of the cell cycle. If the latter were the case then, since S phase is a small portion of the cell cycle, most clones should have a low S-phase index. Instead, the S-phase indexes were broadly distributed (Fig. 2C,D). The level of EdU incorporation also did not correlate with the size of the clone ($r=0.41$, $P=0.2$, Fig. 2C). These results indicate that any synchronization of the cell cycle of clonally related cells is not strong and that each pure oEGL clone might have a distinct proliferation index that varies over time.

Oriented expansion of gcps underlies preferential AP growth of folia

We found a significant AP oriented anisotropy in the growth of the Cb, since at P14 the circumference of the Swiss Webster Cb midline is 7.8 times longer in the AP than ML axis, whereas at E17.5 the AP axis is half the length of the ML axis (supplementary material Fig. S3). We tested whether the geometry of gc clones would reveal any oriented behaviors (proliferation, cell migration or cell dispersion) that underlie the anisotropic growth. We first measured the longest length that each clone occupied along the AP and ML axes (>8 cells and <1024 to ensure single clones) (Fig. 3A). Strikingly, pooling our data from the four groups of clones ($n=149$), 87.9% were more elongated along the AP axis than the ML axis (Fig. 3B). This AP polarized geometry could be due to oriented expansion of proliferating gcps and/or to oriented cell dispersion of postmitotic

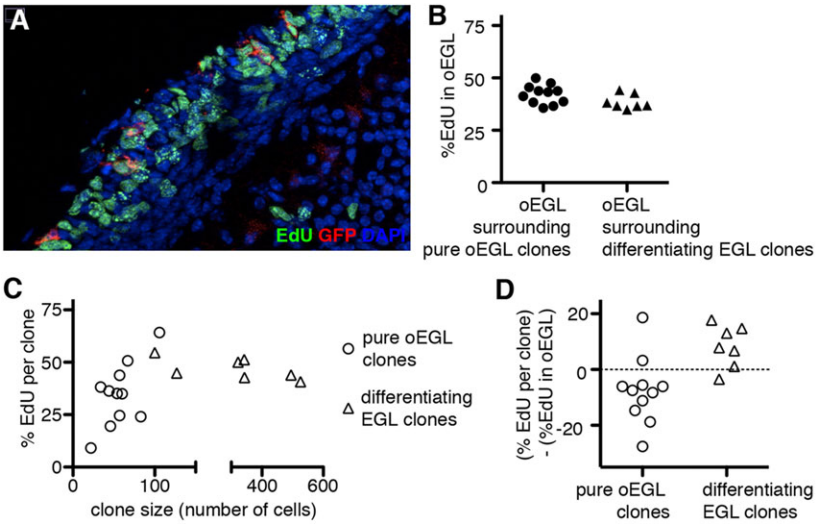

Fig. 2. Clonally related cells are poorly synchronized in cell cycle phase. (A) An E17.5→P7 clone (red) with EdU marking of cells in S phase (green). (B) S phase of oEGL cells surrounding each clone. (C) S phase of two clone types plotted in relation to clone cell number. (D) Difference between the percentage of EdU^+ cells in each clone and in neighboring oEGL cells.

Development (2015) 142, 1661-1671 doi:10.1242/dev.120287

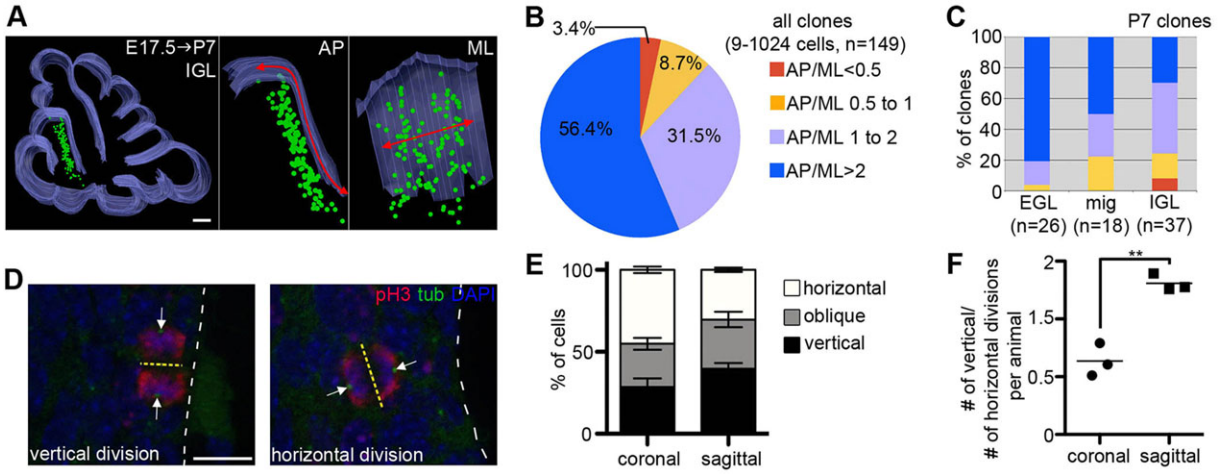

Fig. 3. Clones expand preferentially along the AP axis. (A) Neurolucida 3D representation of an E17.5→P7 IGL clone (left), with AP and ML views (middle and right). Contours of the cerebellum are represented in blue and cells of the clone as green dots. Arrows indicate AP and ML length measurements. Scale bar: 250 µm. (B) AP/ML length rations of each clone. (C) AP/ML ratios of P7 (E15.5→P7 and E17.5→P7) clone subtypes. (D) Examples of anaphase figures showing chromatin (pH3, red), centrosomes (γ-tubulin, green) and DNA (DAPI, blue). Scale bar: 20 µm. Dashed yellow line indicates the plane of division; dashed white line indicates the pial surface; arrows indicate centrosomes. (E) Percentage of cells undergoing the indicated divisions. n=3, >79 cells from three to five sections/animal; error bars indicate s.d. (F) Ratio of vertically versus horizontally dividing cells. n=3; $^{**}P$=0.0019 (t-test).

gcs. Interestingly, by analyzing the E15.5→P7 and E17.5→P7 clones we found that 80.8% of the EGL clones had an AP/ML ratio >2, whereas only 50% of the migrating clones and even fewer (29.7%) of the IGL clones had an AP/ML ratio >2 (Fig. 3C). This result demonstrates that the AP polarized shape of clones is determined during the proliferation of gcps in the EGL, and the polarization diminishes as cells differentiate.

We tested whether AP oriented cell division underlies the preferential AP expansion of EGL clones by visualizing anaphase figures at P4 in whole cerebella. In both coronal and sagittal sections, each cell in anaphase was categorized as a horizontal division (parallel to the EGL surface, 0-30°, Fig. 3D), vertical division (perpendicular to the EGL surface, 60-90°, Fig. 3D) or oblique division (30°-60° to the EGL surface). In coronal sections, vertical divisions should result in addition of cells to the ML axis and in sagittal sections to addition of cells to the AP axis. In both section planes, the horizontal divisions should contribute to thickening of the EGL or partitioning of cells to the iEGL. Horizontal divisions were used as a reference to calculate whether vertical divisions were more frequent along the AP axis than the ML axis. Interestingly, the ratio of vertical/horizontal divisions was significantly higher in sagittal than in coronal sections (P=0.0019, Fig. 3F), revealing that the division plane of gcps is preferentially along the AP axis in the P4 Cb at a stage of extensive proliferation of the EGL. Therefore, AP oriented gcp division is likely to be a key mechanism leading to the prominent AP spread of gcps.

ML expansion of gc clones results from non-polarized tangential migration in the iEGL

We then determined the origin of the decrease in AP/ML ratio as gc clones differentiate at P7 (Fig. 3C). Interestingly, the average AP length of EGL clones was similar to that of migrating clones (P=0.73 in the E15.5→P7 group and P=0.50 in the E17.5→P7 group) (Fig. 4B,C), whereas the ML length of migrating clones was significantly longer than that of EGL clones (P=0.002 and P<0.0001 for E15.5→P7 and E17.5→P7 clones, respectively) (Fig. 4D,E). Concomitantly, the average distance between nearest clonally related cells (dispersion) increased in migrating clones (32.4 µm, or two to three cell diameters) compared with EGL clones (26.2 µm) (P=0.11, Fig. 4A).

Tangential migration in the iEGL is likely to be the major contributor to the ML dispersion of migrating gcs. Indeed, the ML length of the IGL clones, which reflects the full extent of ML tangential migration, was significantly longer than that of migrating clones (P=0.007 and P=0.003 for E15.5→P7 and E17.5→P7 clones, Fig. 4D,E). To determine whether tangential migration occurs preferentially towards medial or lateral positions compared with the initial position of the gcps in the EGL, we examined 11 migrating clones that contained some gcps in the oEGL. Significantly, in 8 of the 11 clones, the migrating gcs covered a greater ML length than the gcps in the oEGL, with gcs being either more lateral (n=3), medial (n=1) or both (n=4) than any of the gcps in the oEGL (data not shown). Therefore, cells within a clone do not all migrate in the same tangential direction in the iEGL, resulting in an overall increase in the ML length of clones.

IGL gcs randomly disperse due to intercalation of newly produced cells

We next examined dispersion within the IGL, where clonally related gcs settle throughout the thickness of the IGL (supplementary material Fig. S1C) (Espinosa and Luo, 2008). Interestingly, the dispersion of gcs in the IGL was greater within adult than P7 clones (77.2 µm versus 64.5 µm), suggesting that newly produced gcs intercalate between gcs that had previously settled in the IGL. This model implies that, at any developmental stage, the earlier a clone has reached the IGL (the clones with fewer cells), the more likely its cells will become dispersed by later born cells. Indeed, the higher the number of cells in an IGL clone, the less dispersed the gcs were (E15.5→P7, r=−0.83, P<0.0001; E17.5→P7, r=−0.78, P<0.0001; E17.5→adult, r=−0.68, P=0.0001; P1→adult, r=−0.68, P<0.0001) (Fig. 5A; data not shown).

We next compared the level of dispersion of E17.5→P7 IGL clones with that of E17.5→adult IGL clones having a similar size range (9-285 cells), reasoning that such small adult IGL clones are likely to have differentiated before P7. Indeed, the five small

Development (2015) 142, 1661-1671 doi:10.1242/dev.120287

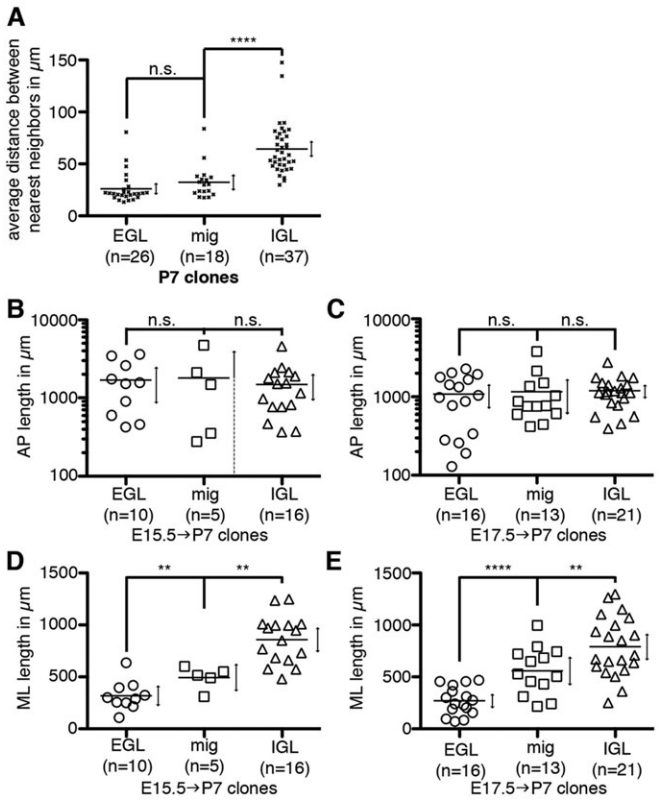

Fig. 4. Migrating and IGL gcs preferentially disperse along the ML axis. (A) Level of dispersion within the three P7 clone subtypes (E15.5→P7 and E17.5→P7). ****P<0.0001. (B,C) AP length of clone subtypes plotted on a $\log_{10}$ scale. (D,E) ML length of the E15.5→P7 (**P=0.002, **P=0.007) or E17.5→P7 EGL (****P<0.0001. **P=0.003) clone subtypes. Mean value (horizontal line) with 95% confidence interval (double vertical arrow) shown. n.s., non-significant (P-values were calculated from linear regression models with generalized estimating equations).

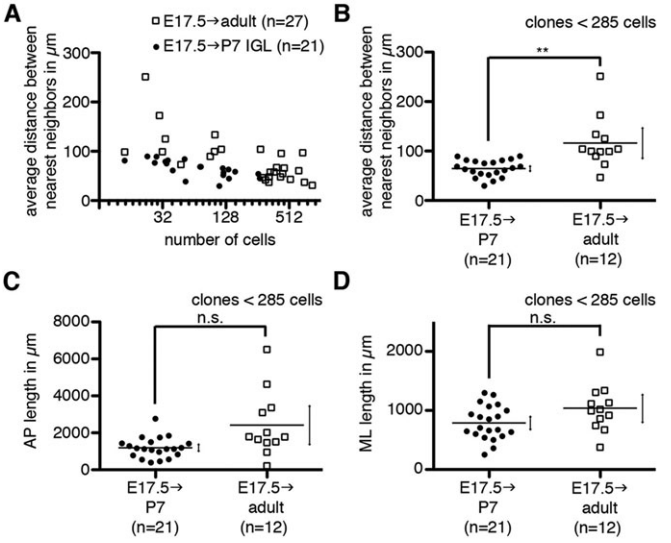

Fig. 5. Later born gcs disperse already differentiated IGL gcs. (A) Level of dispersion of E17.5→P7 and E17.5→adult IGL clones plotted in relation to clone cell number ($\log_2$ scale). (B-D) Level of dispersion (B), AP length (C) and ML length (D) of clones of similar size (9-285 cells). **P=0.002 (P-values were calculated from linear regression models with generalized estimating equations).

E17.5→adult clones in which the position of parallel fibers could be detected had their parallel fibers either in the inner third (n=4) or the inner half (n=1) of the ml (supplementary material Fig. S2D), indicating early differentiation. We found that the gc dispersion in small E17.5→adult IGL clones was significantly greater than in E17.5→P7 IGL clones (P=0.002) (Fig. 5B). However, the AP/ML ratios of the small E17.5→adult and all E17.5→P7 IGL clones were similar (Fig. 5C,D, P=0.14 and P=0.13). Thus, our study has revealed that gc dispersion within the IGL is largely due to intercalation of later born gcs without an obvious polarization.

Gcs do not disperse across the base of fissures

Paralleling the AP anisotropy of gc clones, clones of cerebellar ventricular zone-derived cells (Purkinje, ml and Golgi neurons) were found to be more elongated along the AP than ML axis (Mathis et al., 1997). Interestingly, although such clones dispersed throughout the AP axis, they did not cross the midline. In order to determine whether gcs disperse freely along the AP and ML axes, the positions of the ML and AP limits of each clone (8-1024 cells) were determined in relation to anatomical landmarks. Interestingly, in the ML axis no single point of restriction in cell dispersion was detected for all clone sets between the vermis and hemispheres (supplementary material Fig. S5A-D). Moreover, the midline was not a site of restriction. Therefore, gcs disperse freely along the ML axis.

In the AP axis the most obvious anatomical landmark is the base of each fissure (referred to as ‘base’) and the top of the folia (‘top’). Remarkably, we detected many clones with one of their AP limits close to a base (within 5% of the total length of the folium; n=38/149), whereas few clones had an AP limit close to the top (n=9/149) (supplementary material Fig. S5E-H). We calculated the frequency that clones had an AP limit at 40 evenly spaced positions along the AP axis of each folium (‘border index’, supplementary material Fig. S6). The frequency of clones with a limit close to a fissure base was significantly higher than at any other position (supplementary material Fig. S6), thus suggesting that gc dispersion is specifically restricted at the base of fissures. To further test whether the bases influence gc dispersion, the percentages of clones that crossed through a base, a top, a base and top or did not cross either were calculated (Fig. 6A). Strikingly, the clones induced at or after E17.5, when some fissures have begun to form, were significantly less likely to cross a base than a top (P=0.008), whereas clones initiated before fissures form (E15.5→P7 clones) had a similar percentage of clones that crossed a base and/or a top (Fig. 6A; supplementary material Table S4). This raised the possibility that, as development progresses, gcs cannot disperse through the base of a fissure. This implies that clones induced at E17.5 or P1 should only cross through fissure bases (anchoring centers) that were absent at the time of clone marking.

To test this idea, we determined precisely when each fissure forms at every position along the ML axis of the Cb (Fig. 6B; supplementary material Fig. S7). We then mapped the distribution of clones relative to fissures that had formed around the time of Tm administration. Consistent with our prediction, out of the 18 E17.5→P7, E17.5→adult and P1→adult clones that crossed a base, none crossed a base that was present before or at the time Tm was administered (Fig. 6C) and only five clones crossed a base formed within 24 h after Tm administration (indicated by asterisks in Fig. 6C). To further test this hypothesis, we determined whether fissures that had formed by the time that clone marking was complete (24 h post-Tm) were less likely to be crossed than the

Development (2015) 142, 1661-1671 doi:10.1242/dev.120287

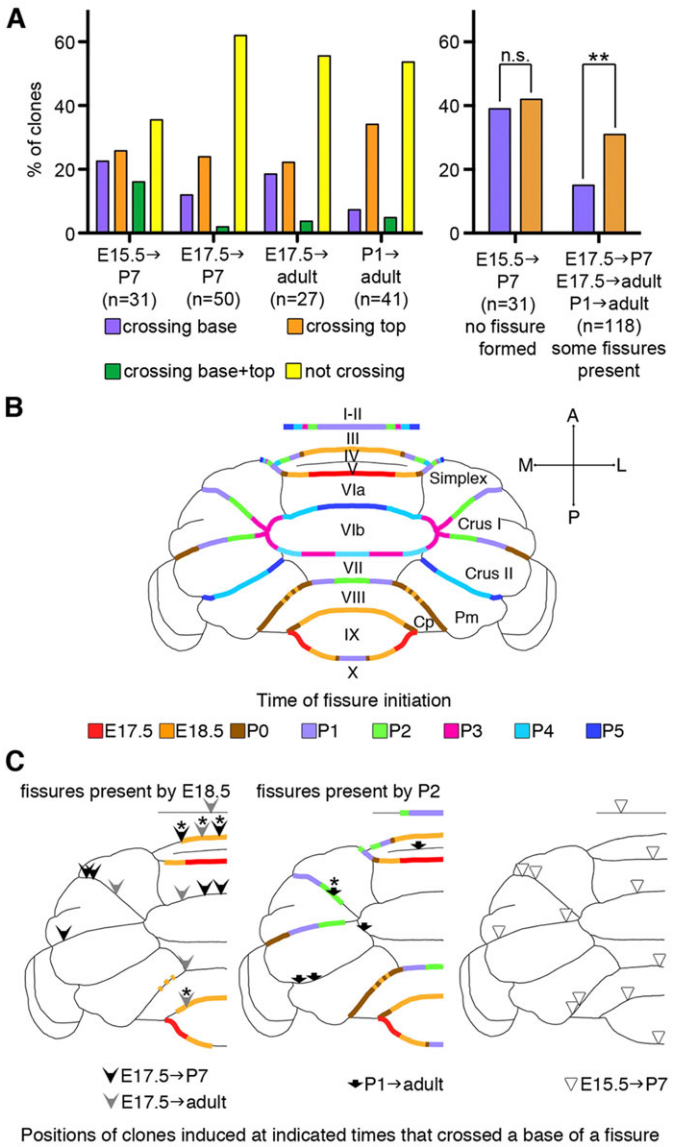

Fig. 6. Cell dispersion is restricted by the bases of the fissures.
(A) Percentage of each clone type (9-1024 cells) with the indicated behaviors (left), and the percentage of clones crossing any fissure base (purple) or any top (orange) for the E15.5 induction time point (when no fissures are formed) and the E17.5 and P1 induction time points (when some fissures are present). **P=0.008 (McNemar's test). (B) Color coding of the timing of fissure formation. The top line represents precentral fissure. (C) The positions of clones are indicated only for those that crossed a fissure base. Fissures that had formed within 24 h of Tm administration and were crossed are indicated by an asterisk. The positions of clones induced at E15.5 (right) that crossed a fissure are shown for comparison. Pm, paramedian; Cp, copula pyramidis.

fissures formed subsequently. Each clone was assigned to its closest fissure, and the E17.5→P7, E17.5→adult and P1→adult clones were found to be evenly distributed between fissures that had (n=54) or had not (n=52) formed when marking was complete. Indeed, the fissures not yet formed at the time of clone marking were crossed significantly more often (n=13/52) than those that had begun forming after the end of clone marking (n=5/54; P=0.03) (supplementary material Fig. S8, Table S2). These results provide strong evidence that once an anchoring center is formed it acts as a barrier to gcp dispersion and, by extrapolation, that gcp clones become confined to specific folia.

The geometry of a gc clone correlates with the size of the folium

Since two adjacent anchoring centers confine clonally related gcs to the intervening folium, a possible mechanism to produce folia of different sizes is differential regulation of the growth characteristics of clones within distinct folia. Consistent with this idea, we found that clones from all four datasets that resided in long folia had significantly more cells than clones in short folia (P=0.007, Fig. 7A-C). However, the level of cell dispersion in both groups of clones was similar (P=0.99, Fig. 7D). The clones in long folia also had a significantly greater AP/ML ratio (P<0.0001, Fig. 7E). These distinct clone geometries and cell numbers correlate with the more extended AP axis of long folia.

The greater AP/ML ratio of the clones in long folia could simply be due to the fact that clones in long folia have more cells than clones in short folia. To test this hypothesis, clones in long folia were divided into two groups: large clones (>150 and <1024 cells) and small clones with a similar range of cell numbers to short folia (>8 and <150 cells). We found that large and small clones in long folia had similar AP/ML ratios (P=0.46, Fig. 7F). Moreover, clones in short folia had a significantly lower AP/ML ratio (P<0.0001) and shorter AP length (P<0.0001) than the small clones in long folia (Fig. 7F,G), whereas their ML lengths were similar (P=0.31, Fig. 7H). Therefore, the strong AP elongation of the clones in long folia does not correlate with their cell number but might be an intrinsic property of the growth characteristics of the clones.

Clone cell number and geometry are altered in *En1*$^{+/-}$;*En2*$^{-/-}$ mutants

A prediction of our model, whereby differential regulation of gc behaviors determines the size of folia, is that in mutants with a diminished Cb the clone geometry should be similar to that in WT small folia. We generated E17.5→adult gcp clones in *En1*$^{+/-}$;*En2*$^{-/-}$ mice (Fig. 8; supplementary material Table S5), which have an abnormal foliation pattern and shorter folia (Fig. 8A,B) (Sgaier et al., 2007), and compared them with the WT clones. We first tested whether the smaller mutant Cb is a consequence of gcps in *En1*$^{+/-}$;*En2*$^{-/-}$ mutants dividing less frequently than in WT after E17.5 or is due to fewer gcps being present at E17.5 but which divide normally. Consistent with the former, the clones in *En1*$^{+/-}$;*En2*$^{-/-}$ mutants had significantly fewer cells than WT clones (average of 197 versus 446.3 cells, P=0.01, Fig. 8C). Interestingly, the AP/ML ratio was reduced in the mutant gc clones compared with WT (P=0.05, Fig. 8E), whereas the overall dispersion of the cells within clones was comparable to WT (P=0.57, Fig. 8D). Although both the AP and ML lengths of the mutant clones were significantly reduced compared with WT (P=0.02 and P=0.03, respectively), the AP length was reduced to a greater extent, accounting for the AP/ML ratio being significantly reduced (Fig. 8F,G). Thus, *En1*$^{+/-}$;*En2*$^{-/-}$ clones have a reduced degree of AP anisotropy compared with WT clones.

We next tested whether the reduced AP/ML ratio of *En1*$^{+/-}$;*En2*$^{-/-}$ clones compared with WT was simply due to their reduced cell number. We found, however, that the AP lengths of 'small WT clones' with the same cell number range as *En1*$^{+/-}$;*En2*$^{-/-}$ clones (>8 and <285) were greater than those of the mutant clones (2417.7 µm versus 1429.8 µm, Fig. 8F,G). Although this difference was not statistically significant using the entire WT dataset (P=0.23), when the outlier WT clone that clearly had a much shorter AP length than any other WT clones

Development (2015) 142, 1661-1671 doi:10.1242/dev.120287

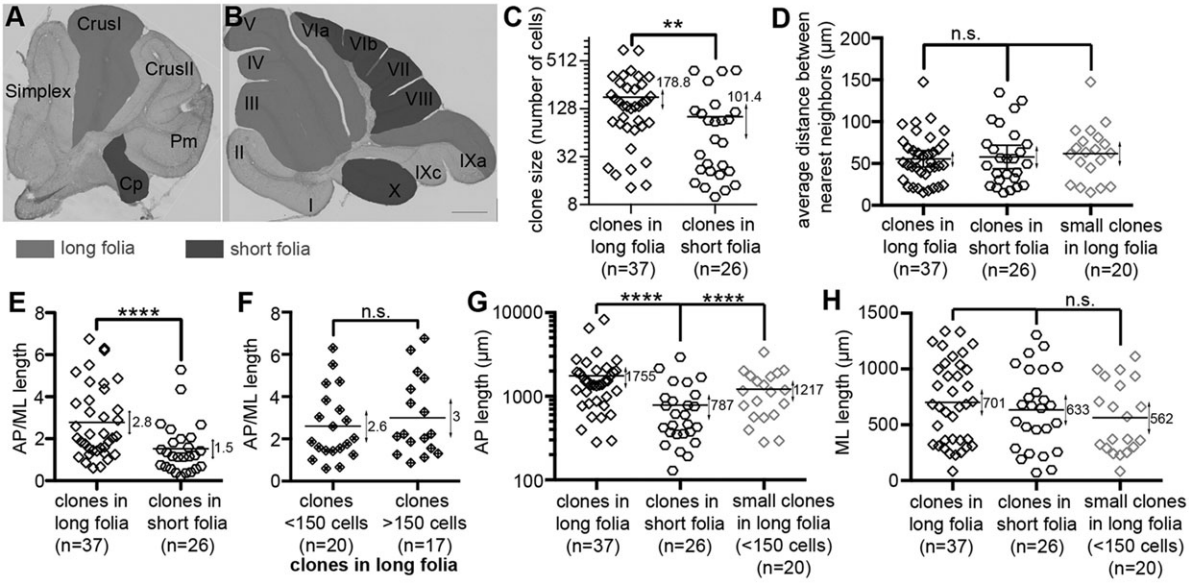

Fig. 7. AP/ML length ratio and clone cell number are greater in long than in short folia. (A,B) Sagittal sections of (A) hemisphere and (B) midline vermis with long and short folia indicated. Scale bar: 500 µm. (C-H) The number of cells (C), level of dispersion (D), AP/ML length ratio (E,F), AP length (G) and ML length (H) of the indicated clones in long and short folia. The mean value (horizontal line) and 95% confidence interval (vertical double arrow) are shown. ****P<0.0001, **P=0.007 (the P-value for C was calculated from a Poisson regression model with generalized estimating equations; for the other panels, P-values were calculated from linear regression models with generalized estimating equations).

(and thus could be a spontaneous clone) was removed, the average AP length of the small WT clones was significantly longer than that of the $En1^{+/-};En2^{-/-}$ clones (P=0.002), whereas the ML length was not. Therefore, the reduction in the AP length of gc clones in $En1^{+/-};En2^{-/-}$ mutants is not only due to a decrease in the number of cells that are produced or survive in each clone, but, similar to WT clones in short folia, is also due to a change in the behavior of the gcps and/or gcs that alters clone geometry.

DISCUSSION

Our clonal analysis in the mouse Cb has uncovered a new dimension to the anchoring center as a structure that limits gcp dispersion (Ma et al., 2012; Sudarov and Joyner, 2007). This property has major implications for the process of foliation, as compartmentalization of the Cb could provide a means to shape folia by allowing differential regulation of gcp behaviors in each folium. Indeed, we uncovered that fine tuning of the plane of cell division, number of cell divisions and polarity of

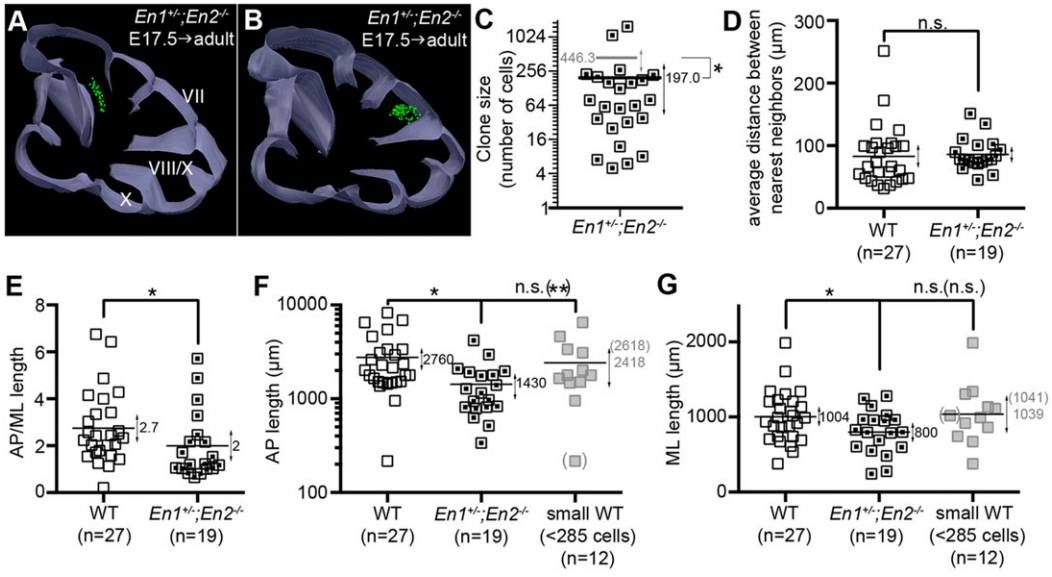

Fig. 8. Clones are smaller and less extended along the AP axis in $En1^{+/-};En2^{-/-}$ mutants. (A,B) Neurolucida 3D reconstruction of E17.5→adult $En1^{+/-};En2^{-/-}$ clones. (C) Size of each $En1^{+/-};En2^{-/-}$ clone ($\log_2$ scale). Gray line indicates the mean size of WT E17.5→adult clones (*P=0.01, n=19 mutant clones; P-value was calculated from a Poisson regression model with generalized estimating equations). (D-G) The level of dispersion (D), AP/ML ratio (*P=0.05) (E), AP length (*P=0.02, **P=0.002 excluding the outlier) (F) and ML length (*P=0.03) (G) of each WT and $En1^{+/-};En2^{-/-}$ clone type. Mean values (horizontal black lines) with 95% confidence interval (double vertical arrows) are shown. The parentheses in F and G indicate the WT outlier clone or statistical tests (P-values were calculated from linear regression models with generalized estimating equations) calculated with the outlier excluded.

Development (2015) 142, 1661-1671 doi:10.1242/dev.120287

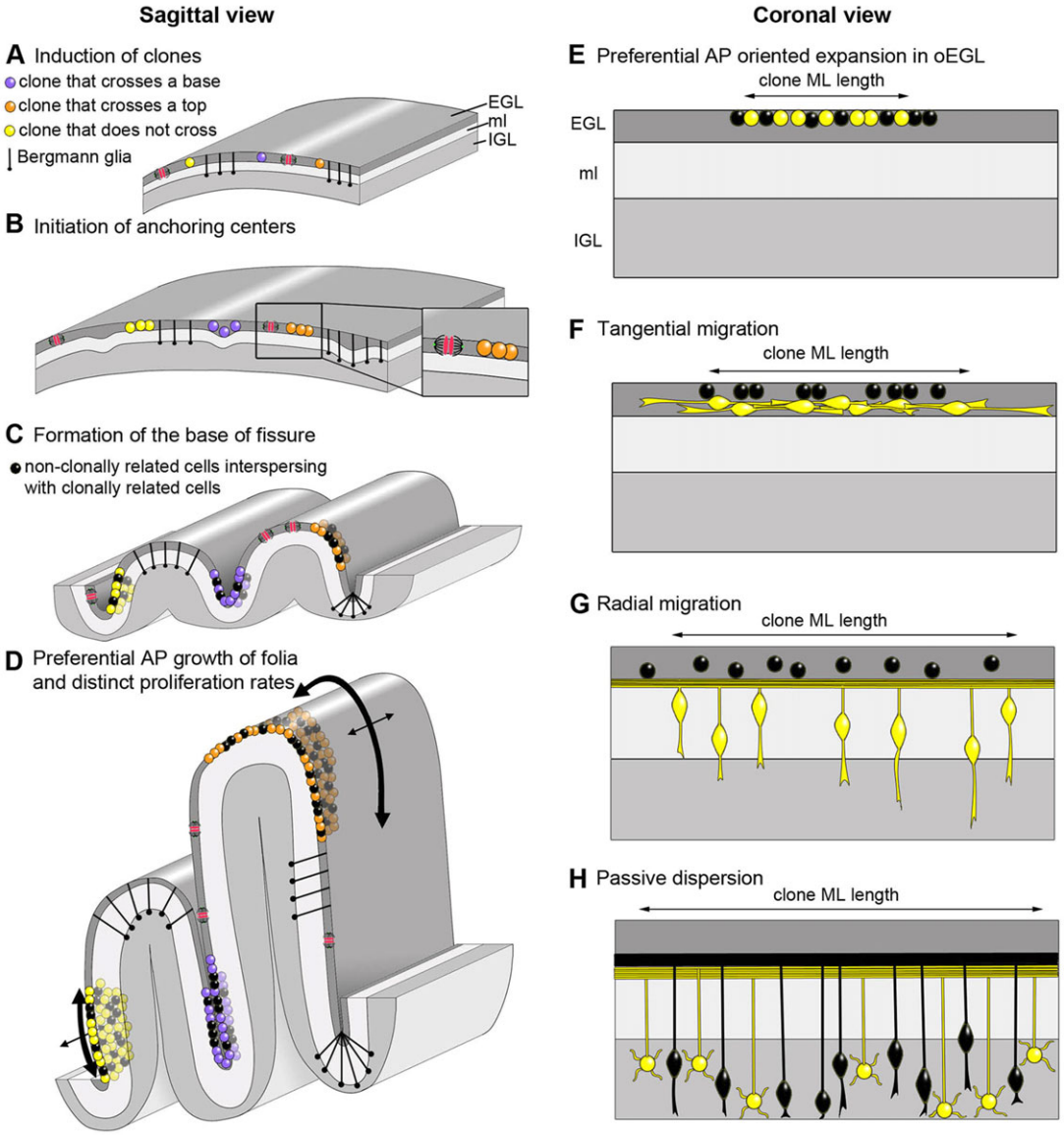

Fig. 9. Schematic representation of gc behaviors that determine the shape of cerebellar folia. (A-D) Three clones marked at E15.5 that represent a clone that initially spans a fissure base (purple), is beside a base (yellow) or at the top of a folium (orange) are shown before (A) or after (B-D) fissures have formed. All clones expand more along the AP than ML axis (double arrows), but clones in long folia have more cells and a greater AP/ML length ratio. Radial processes of Bergmann glia are shown converging at the base of a fissure. The division plane is preferentially oriented along the AP axis (inset in B shows mitotic figures). (E-H) Clonally related gcs (yellow) undergo synchronized successive cell movements and gc parallel fibers stack in an inside to outside temporal manner.

dispersion in each folium could contribute to the final geometry of gcp clones and account for the differences that we observed in long versus short WT folia and in *En1*$^{+/-}$;*En2*$^{-/-}$ Cb. We propose a model for how gcp behaviors determine the Cb foliation pattern (Fig. 9).

Clonally related gcps are not well synchronized in cell cycle phase

Given that all gcps of a clone exit the cell cycle within a narrow time window (Espinosa and Luo, 2008) (the present study), we tested whether clonally related gcps are synchronized in their phase of the cell cycle. In contrast to randomly sampled gcps that show little variation in the S-phase index (±4%) or differentiating clones (±5.1%), we found that pure oEGL clones have a much higher degree of variation (±15.2%). Although it is possible that the cell cycle phase of cells within a clone is partially synchronized, we favor the hypothesis that each clone has a distinct rate of proliferation that changes over time. First, most clones did not have a low S-phase index, contrary to what would be predicted for synchronized clones. Second, the two clones with the highest and lowest S-phase indexes had the greatest and least cells, respectively, although this correlation was not true for all clones. Therefore, the final size of a gc clone is likely to be dictated by its cumulative and changing proliferation rate. An intriguing question is how clonally related cells sense each other and differentiate together within a day.

Proliferating gcps drive a massive AP expansion of the Cb, while migrating gcs modestly expand the ML axis

Strikingly, we found that the circumference of the cerebellar medial AP axis increases 17.6-fold between E17.5 and P14 compared with

Development (2015) 142, 1661-1671 doi:10.1242/dev.120287

only a 2.2-fold increase in the ML axis (supplementary material Fig. S3). Correlating with this polarized growth, we discovered a remarkable anisotropy in the geometry of gcp/gc clones: 56.4% of clones were >2-fold longer in the AP than ML axis. Whereas gcp clones marked by retroviral labeling of the rhombic lip (Ryder and Cepko, 1994) were all of similar shape due to migration over the surface of the cerebellar primordium, we discovered a strong AP bias in the growth of gcp clones after their AP migration from the rhombic lip is complete, as ∼80% of EGL-only clones are strongly AP elongated. By contrast, migrating clones increase their ML length and gcs in the IGL increase in both directions. Tangential migration of gcs in the iEGL must account for the increase in ML length, as radial migration should not alter clone shape (Komuro et al., 2001). As we found that the ML length of clones increases, gcs within a clone must randomly migrate medially or laterally rather than all migrating in one direction. It has been shown that when gcs enter the IGL they actively migrate (Hippenmeyer et al., 2010; Komuro and Rakic, 1998). We uncovered that there is an additional phase of apparently passive dispersion of gcs in the IGL due to intercalation of later born gcs.

In summary, gcps first undergo a phase of AP oriented expansion, then migrating gcs in the iEGL undergo active non-polarized expansion along the ML axis, and finally gcs in the IGL disperse randomly due to intercalation of newly differentiated gcs (Fig. 9).

AP oriented gcp cell division underlies the massive AP expansion of the Cb

We discovered a preferential AP orientation to gcp cell division when analyzed at P4. The ratio between AP and ML oriented cell divisions may change over time; however, the bias that we observed at P4, when the EGL is highly proliferative, strongly suggests that the orientation of cell divisions is a contributor to the biased AP expansion of the clones and thus provides a cellular basis for the massive AP expansion of the Cb. Although gc migration has been extensively studied (Famulski et al., 2010; Solecki et al., 2006, 2009), little is known about potential polarity signals in the EGL that could drive oriented cell divisions. One possibility is that the early expression of genes in AP stripes, such as *En1*, *En2*, *Pax2*, *Wnt7b* (Millen et al., 1995) and *Epha4* (Karam et al., 2000), provides positional clues for the orientation of gcp cell division. Another is that mechanical constraints are conferred through adhesion processes (Blaess et al., 2004; Sievers et al., 1981). Of possible relevance, Gap43, an actin-binding phosphoprotein, has been proposed to provide a link between the orientation of the mitotic spindle of gcps and extrinsic cues, as gcps lacking Gap43 have an altered orientation of mitotic spindles and more frequent horizontal than vertical divisions (Mishra et al., 2008). Interestingly, *Gap43* null mutants have shorter folia than normal (Shen et al., 2008). The proportions of AP and ML vertical divisions in the mutants were not examined, so it remains unclear whether a change contributes to the phenotype. Studies in *Antirrhinum* have shown that genetically controlled local changes in growth rates or the direction of growth can generate differently shaped petals, suggesting that cell behaviors can indeed influence morphology (Green et al., 2010). Clonal analysis of marked mutant clones, using systems such as MADM (Zong et al., 2005) or MASTR (Lao et al., 2012), will be crucial for teasing out the processes underlying the polarization of gcp cell divisions.

Anchoring centers restrict the dispersion of gcps and drive foliation

Perhaps the most unanticipated finding of our clonal analysis of WT cells is that clonally related gcs are confined to individual folia. Gcs within a clone are not restricted to one folium from the start of foliation; instead, as fissures progressively form, the territory that they can occupy is gradually restricted to between fissures. The anchoring centers at the base of each fissure are sites of highly specific behaviors of several cerebellar cell types (Ma et al., 2012; Sudarov and Joyner, 2007), including a transient increase in gcp proliferation, radial elongation of the gcp body and a fanning out of gcs as they migrate along the Bergmann glial fibers that radiate out from the fissure base (Sudarov and Joyner, 2007) (Fig. 9C,D). One possibility is that anchoring centers impose a mechanical constraint on gcps that prevents their dispersion between folia. Such a feature of anchoring centers could be key to cerebellar foliation. Since gcps cannot cross the anchoring centers, newly formed gcps might be forced away from the base of fissures causing the outward bulge of a fold.

Do folds act as developmental units?

The confinement of clonally related cells within a folium is reminiscent of developmental compartments (Fraser et al., 1990; Garcia-Bellido et al., 1973; Vincent, 1998) in which progeny are prevented from entering the neighboring territory by a lineage boundary, and which have a distinct gene expression signature and cellular functions. Although we showed that in the Cb the base of each fissure is a lineage boundary and, as was previously hypothesized (Welker, 1990), that each folium is likely to act as a functional compartment, no specific markers have been identified that delineate each folium. We propose that the folia constitute developmental units, if not compartments per se. Consistent with this, we found that gc clones have different properties depending on the size of the folium that they occupy, with long folia containing clones with greater dimensions, cell number and AP/ML ratio than short folia. Furthermore, in $En1^{+/-};En2^{-/-}$ mutants, which have a smaller Cb primarily along the AP axis, gc clones have similar properties to WT clones in short folia. This difference in gc behavior in WT small folia and *En1/2* mutants as compared with WT long folia could be due to differential intrinsic properties regulating the orientation of cell division or to differential extrinsic constraints that influence cell division orientation. However, the highly conserved WT pattern of foliation suggests that there is regulation at the genetic level (Altman and Bayer, 1997; Larsell, 1970). We hypothesize that anchoring centers not only play a structural role in foliation, but also provide a means for differentially regulating specific gcp behaviors at the genetic level in each folium, and thus ultimately contribute to the diversity of folial size and shape.

In a recent study of neocortex folding, it was proposed that the fibers of a group of basal radial glial cells spread out like a fan and direct the migration of neurons laterally creating the folds (gyri) (Stahl et al., 2013). Our studies in the cerebellar cortex raise the possibility of a different or additional model. We propose that a critical first step in folding of the neocortex is the production of groups of basal radial glia cell bodies that are able to fan out in a semicircle because they have detached from the apical surface and their basal fibers converge on one point in the pial surface like the spokes of a wheel. The hub of the wheel would form the base of the fold (sulcus), like the anchoring centers of the Cb with their associated Bergmann glial fibers (Fig. 9C,D). The surface of the cortex would bulge outward between the hubs during neurogenesis, creating the gyri. It will be important to determine whether neural progenitor behaviors in gyrencephalic mammals are differentially regulated in distinct neocortex folds. Finally, as the number of cells in the Cb and neocortex have scaled together during evolution, along with a selective expansion of cerebellar folia connected to

Development (2015) 142, 1661-1671 doi:10.1242/dev.120287

prefrontal cortex circuits from simian to human (Balsters et al., 2010; Herculano-Houzel, 2010), the spatial segregation of neurons into folia might have played a crucial role in the coordinated expansion and co-evolution of functionally connected circuits in the two brain regions.

MATERIALS AND METHODS

Mouse lines

The *Atoh1-CreER^{T2}* (Machold and Fishell, 2005), *R26R^{YFP}* (Srinivas et al., 2001), *En1^{hd}* (Wurst et al., 1994) and *En2^{ntd}* (Millen et al., 1994) mouse lines were maintained on an outbred Swiss Webster background and genotyped as previously described. All animal studies were performed under an approved Institutional Animal Care and Use Committee mouse protocol according to MSKCC institutional guidelines. Noon of the day that a vaginal plug was detected was designated as E0.5. The equivalent of E19.5 is referred to as P0.

Clonal marking of gcps

WT *Atoh1-CreER^{T2}/+;R26R$^{YFP/+}$* mice and *Atoh1-CreER^{T2}/+;R26R$^{YFP/+}$;En1$^{+/hd}$;En2$^{ntd/ntd}$* mutants were used for the generation of clones. Tm diluted in corn oil (0.5-1.75 µg/g body weight) was administered by intraperitoneal injection of pregnant females or subcutaneous injection of P1 pups as described (Legué and Joyner, 2010).

Histology and immunohistochemistry

Brains were dissected after intracardiac perfusion and postfixed in 4% PFA for 2 h at 4°C, then transferred into 30% sucrose. P7 brains were embedded in OCT (Tissue-Tek), frozen in methyl-butane and cryosectioned at 12 µm for clonal analysis at P7, or 20 µm for cell division analysis and 40 µm (free-floating) for adult analysis. Brains were serially sectioned and any missing sections were recorded for quantitative analysis. Immunohistochemistry for GFP was performed following standard protocols (Legué and Joyner, 2010).

EdU analysis

10 mg/ml EdU in PBS was injected subcutaneously (100 µg/g body weight) 30 min before euthanizing P7 mice. EdU was detected using the Click-iT EdU Alexa Fluor 488 Imaging Kit (Invitrogen, C-10337).

Cell division orientation analysis

Anaphase figures were detected using phospho-histone H3 (pH3) antibody [Millipore (Chemicon), 06-570, 1:500] staining. Centrosome position was defined by an indentation of the pH3-DAPI staining or by detection of γ-tubulin using mouse anti-γ-tubulin antibody (Santa Cruz, sc-51715, 1:500). Alexa Fluor 555-donkey anti-rabbit (Invitrogen, A-31572,1:500) and Alexa Fluor 488-donkey anti-mouse (Invitrogen, A-21202, 1:500) secondary antibodies were used. The plane of division was determined as perpendicular to the line between the two centrosomes. The angle between the pial surface of the EGL and the plane of division of the cell was then measured. The angle of division was only measured in the vermis, and the analysis of coronal sections was restricted to the region where the section angle is perpendicular to the pial surface (folia VII-X).

Microscopy

Bright-field and fluorescence images were taken on a Zeiss inverted microscope (Observer.Z1) using Axiovision software (Zeiss). *z*-stacks of optical images were taken with an Apotome system (Zeiss) at a 0.75 µm section interval using a 40× objective for EdU-YFP double staining and at a 0.5 µm section interval using a 63× oil objective for pH3 and γ-tubulin staining. Bright-field images of Nissl staining and YFP (DAB) staining were taken using the Mosaix module of the Axiovision software with a 10× objective.

Three-dimensional reconstruction and analysis of clones in the Cb

The position of cells of each clone was reconstructed in a 3D representation (Fig. 3; supplementary material Fig. S4) of each Cb derived from serial sagittal sections using Neurolucida software (MBF Bioscience) operating a computer-driven stage attached to a Zeiss upright microscope (M1). Contours of the surface of the sections were used to reconstruct the volume of the Cb and each cell was marked by a dot and placed in the appropriate *z*-position. Cell counting, nearest-neighbor analysis and measurement of the AP and ML length of the clones were performed using Neurolucida.

Quantification of the timing of fissure formation

Cerebella were collected every day between E17.5 and P5 (n=3 or 4 at each stage), cryosectioned in series at 12 µm and every sixth slide Nissl stained. Whether fissures were present at each ML position (every 72 µm) was recorded (supplementary material Fig. S6).

Statistical analyses

Comparisons between categorical variables were assessed using either the modified Rao-Scott chi-square test or McNemar's test. Correlations between continuous variables were estimated using the Spearman rank correlation coefficient. Differences between clone sizes were examined using Poisson regression with generalized estimating equations to account for correlations within mice. Differences between continuous variables were examined using linear regression with generalized estimating equations to account for correlations within mice. Differences between variances were assessed using the folded form of the F statistic. For variables with skewed distributions, a log transformation was performed prior to statistical analysis. Analyses were performed using SAS version 9.2 (SAS Institute, Cary, NC, USA).

Acknowledgements

We thank Drs Machold and Costantini for providing the *Atoh1-CreER^{T2}* and *R26R^{YFP}* lines; Drs Ayoub and Rakic for providing access to their microscope and Neurolucida software; Jennifer Polo, Rowena Turnbull and Daniel Stephen for technical support; Drs Espinosa and Luo for sharing unpublished data and helpful discussions; and Drs Espinosa, Lawton, Nicolas, Shi, Sudarov and Willett for critical reading of the manuscript.

Competing interests

The authors declare no competing or financial interests.

Author contributions

A.L.J. and E.L. designed the experiments and wrote the article; E.L. performed the experiments; E.R. performed the statistical analyses.

Funding

This work was supported by the National Institutes of Health [grant MH085726]. Deposited in PMC for release after 12 months.

Supplementary material

Supplementary material available online at
http://dev.biologists.org/lookup/suppl/doi:10.1242/dev.120287/-/DC1

References

Altman, J. and Bayer, S. A. (1997). *Development of the Cerebellar System: In Relation to its Evolution, Structure, and Functions*. Boca Raton, FL: CRC Press.

Altman, J., Anderson, W. J. and Wright, K. A. (1969). Early effects of x-irradiation of the cerebellum in infant rats: decimation and reconstitution of the external granular layer. *Exp. Neurol.* **24**, 196-216.

Balsters, J. H., Cussans, E., Diedrichsen, J., Phillips, K. A., Preuss, T. M., Rilling, J. K. and Ramnani, N. (2010). Evolution of the cerebellar cortex: the selective expansion of prefrontal-projecting cerebellar lobules. *Neuroimage* **49**, 2045-2052.

Blaess, S., Graus-Porta, D., Belvindrah, R., Radakovits, R., Pons, S., Littlewood-Evans, A., Senften, M., Guo, H., Li, Y., Miner, J. H. et al. (2004). Beta1-integrins are critical for cerebellar granule cell precursor proliferation. *J. Neurosci.* **24**, 3402-3412.

Bohn, M. C. and Lauder, J. M. (1980). Cerebellar granule cell genesis in the hydrocortisone-treated rat. *Dev. Neurosci.* **3**, 81-89.

Brownell, I., Guevara, E., Bai, C. B., Loomis, C. A. and Joyner, A. L. (2011). Nerve-derived sonic hedgehog defines a niche for hair follicle stem cells capable of becoming epidermal stem cells. *Cell Stem Cell* **8**, 552-565.

Chédotal, A. (2010). Should I stay or should I go? Becoming a granule cell. *Trends Neurosci.* **33**, 163-172.

Cheng, Y., Sudarov, A., Szulc, K. U., Sgaier, S. K., Stephen, D., Turnbull, D. H. and Joyner, A. L. (2010). The Engrailed homeobox genes determine the different foliation patterns in the vermis and hemispheres of the mammalian cerebellum. *Development* **137**, 519-529.

Corrales, J. D., Blaess, S., Mahoney, E. M. and Joyner, A. L. (2006). The level of sonic hedgehog signaling regulates the complexity of cerebellar foliation. *Development* **133**, 1811-1821.
Espinosa, J. S. and Luo, L. (2008). Timing neurogenesis and differentiation: insights from quantitative clonal analyses of cerebellar granule cells. *J. Neurosci.* **28**, 2301-2312.
Famulski, J. K., Trivedi, N., Howell, D., Yang, Y., Tong, Y., Gilbertson, R. and Solecki, D. J. (2010). Siah regulation of Pard3A controls neuronal cell adhesion during germinal zone exit. *Science* **330**, 1834-1838.
Fraser, S., Keynes, R. and Lumsden, A. (1990). Segmentation in the chick embryo hindbrain is defined by cell lineage restrictions. *Nature* **344**, 431-435.
Fujita, S. (1967). Quantitative analysis of cell proliferation and differentiation in the cortex of the postnatal mouse cerebellum. *J. Cell Biol.* **32**, 277-287.
Garcia-Bellido, A., Ripoll, P. and Morata, G. (1973). Developmental compartmentalisation of the wing disk of Drosophila. *Nat. New Biol.* **245**, 251-253.
Green, A. A., Kennaway, J. R., Hanna, A. I., Bangham, J. A. and Coen, E. (2010). Genetic control of organ shape and tissue polarity. *PLoS Biol.* **8**, e1000537.
Herculano-Houzel, S. (2010). Coordinated scaling of cortical and cerebellar numbers of neurons. *Front. Neuroanat.* **4**, 12.
Hippenmeyer, S., Youn, Y. H., Moon, H. M., Miyamichi, K., Zong, H., Wynshaw-Boris, A. and Luo, L. (2010). Genetic mosaic dissection of Lis1 and Ndel1 in neuronal migration. *Neuron* **68**, 695-709.
Karam, S. D., Burrows, R. C., Logan, C., Koblar, S., Pasquale, E. B. and Bothwell, M. (2000). Eph receptors and ephrins in the developing chick cerebellum: relationship to sagittal patterning and granule cell migration. *J. Neurosci.* **20**, 6488-6500.
Kennaway, R., Coen, E., Green, A. and Bangham, A. (2011). Generation of diverse biological forms through combinatorial interactions between tissue polarity and growth. *PLoS Comput. Biol.* **7**, e1002071.
Komuro, H. and Rakic, P. (1995). Dynamics of granule cell migration: a confocal microscopic study in acute cerebellar slice preparations. *J. Neurosci.* **15**, 1110-1120.
Komuro, H. and Rakic, P. (1998). Distinct modes of neuronal migration in different domains of developing cerebellar cortex. *J. Neurosci.* **18**, 1478-1490.
Komuro, H. and Yacubova, E. (2003). Recent advances in cerebellar granule cell migration. *Cell. Mol. Life Sci.* **60**, 1084-1098.
Komuro, H., Yacubova, E., Yacubova, E. and Rakic, P. (2001). Mode and tempo of tangential cell migration in the cerebellar external granular layer. *J. Neurosci.* **21**, 527-540.
Lao, Z., Raju, G. P., Bai, C. B. and Joyner, A. L. (2012). MASTR: a technique for mosaic mutant analysis with spatial and temporal control of recombination using conditional floxed alleles in mice. *Cell Rep.* **2**, 386-396.
Larsell, O. (1952). The morphogenesis and adult pattern of the lobules and fissures of the cerebellum of the white rat. *J. Comp. Neurol.* **97**, 281-356.
Larsell, O. (1970). *The Comparative Anatomy and Histology of the Cerebellum from Monotremes through Apes*. Minneapolis, MN: University of Minnesota Press.
Legué, E. and Joyner, A. L. (2010). Genetic fate mapping using site-specific recombinases. *Methods Enzymol.* **477**, 153-181.
Legue, E., Sequeira, I. and Nicolas, J.-F. (2010). Hair follicle renewal: authentic morphogenesis that depends on a complex progression of stem cell lineages. *Development* **137**, 569-577.
Lewis, P. M., Gritli-Linde, A., Smeyne, R., Kottmann, A. and McMahon, A. P. (2004). Sonic hedgehog signaling is required for expansion of granule neuron precursors and patterning of the mouse cerebellum. *Dev. Biol.* **270**, 393-410.
Ma, S., Kwon, H. J. and Huang, Z. (2012). Ric-8a, a guanine nucleotide exchange factor for heterotrimeric G proteins, regulates bergmann glia-basement membrane adhesion during cerebellar foliation. *J. Neurosci.* **32**, 14979-14993.
Machold, R. and Fishell, G. (2005). Math1 is expressed in temporally discrete pools of cerebellar rhombic-lip neural progenitors. *Neuron* **48**, 17-24.
Mathis, L., Bonnerot, C., Puelles, L. and Nicolas, J. F. (1997). Retrospective clonal analysis of the cerebellum using genetic laacZ/lacZ mouse mosaics. *Development* **124**, 4089-4104.
Millen, K. J., Wurst, W., Herrup, K. and Joyner, A. L. (1994). Abnormal embryonic cerebellar development and patterning of postnatal foliation in two mouse Engrailed-2 mutants. *Development* **120**, 695-706.
Millen, K. J., Hui, C. C. and Joyner, A. L. (1995). A role for En-2 and other murine homologues of Drosophila segment polarity genes in regulating positional information in the developing cerebellum. *Development* **121**, 3935-3945.
Mishra, R., Gupta, S. K., Meiri, K. F., Fong, M., Thostrup, P., Juncker, D. and Mani, S. (2008). GAP-43 is key to mitotic spindle control and centrosome-based polarization in neurons. *Cell Cycle* **7**, 348-357.
Noguchi, K. K., Walls, K. C., Wozniak, D. F., Olney, J. W., Roth, K. A. and Farber, N. B. (2008). Acute neonatal glucocorticoid exposure produces selective and rapid cerebellar neural progenitor cell apoptotic death. *Cell Death Differ.* **15**, 1582-1592.
Nonaka-Kinoshita, M., Reillo, I., Artegiani, B., Ángeles Martínez-Martínez, M., Nelson, M., Borrell, V. and Calegari, F. (2013). Regulation of cerebral cortex size and folding by expansion of basal progenitors. *EMBO J.* **32**, 1817-1828.
Orvis, G. D., Hartzell, A. L., Smith, J. B., Barraza, L. H., Wilson, S. L., Szulc, K. U., Turnbull, D. H. and Joyner, A. L. (2012). The engrailed homeobox genes are required in multiple cell lineages to coordinate sequential formation of fissures and growth of the cerebellum. *Dev. Biol.* **367**, 25-39.
Ryder, E. F. and Cepko, C. L. (1994). Migration patterns of clonally related granule cells and their progenitors in the developing chick cerebellum. *Neuron* **12**, 1011-1029.
Sgaier, S. K., Lao, Z., Villanueva, M. P., Berenshteyn, F., Stephen, D., Turnbull, R. K. and Joyner, A. L. (2007). Genetic subdivision of the tectum and cerebellum into functionally related regions based on differential sensitivity to engrailed proteins. *Development* **134**, 2325-2335.
Shen, Y., Mishra, R., Mani, S. and Meiri, K. F. (2008). Both cell-autonomous and cell non-autonomous functions of GAP-43 are required for normal patterning of the cerebellum in vivo. *Cerebellum* **7**, 451-466.
Sievers, J., Mangold, U., Berry, M., Allen, C. and Schlossberger, H. G. (1981). Experimental studies on cerebellar foliation. I. A qualitative morphological analysis of cerebellar fissuration defects after neonatal treatment with 6-OHDA in the rat. *J. Comp. Neurol.* **203**, 751-769.
Sillitoe, R. V. and Joyner, A. L. (2007). Morphology, molecular codes, and circuitry produce the three-dimensional complexity of the cerebellum. *Annu. Rev. Cell Dev. Biol.* **23**, 549-577.
Solecki, D. J., Govek, E.-E. and Hatten, M. E. (2006). mPar6 alpha controls neuronal migration. *J. Neurosci.* **26**, 10624-10625.
Solecki, D. J., Trivedi, N., Govek, E.-E., Kerekes, R. A., Gleason, S. S. and Hatten, M. E. (2009). Myosin II motors and F-actin dynamics drive the coordinated movement of the centrosome and soma during CNS glial-guided neuronal migration. *Neuron* **63**, 63-80.
Srinivas, S., Watanabe, T., Lin, C.-S., William, C. M., Tanabe, Y., Jessell, T. M. and Costantini, F. (2001). Cre reporter strains produced by targeted insertion of EYFP and ECFP into the ROSA26 locus. *BMC Dev. Biol.* **1**, 4.
Stahl, R., Walcher, T., De Juan Romero, C., Pilz, G. A., Cappello, S., Irmler, M., Sanz-Aquela, J. M., Beckers, J., Blum, R., Borrell, V. et al. (2013). Trnp1 regulates expansion and folding of the mammalian cerebral cortex by control of radial glial fate. *Cell* **153**, 535-549.
Sudarov, A. and Joyner, A. L. (2007). Cerebellum morphogenesis: the foliation pattern is orchestrated by multi-cellular anchoring centers. *Neural. Dev.* **2**, 26.
Vincent, J. P. (1998). Compartment boundaries: where, why and how? *Int. J. Dev. Biol.* **42**, 311-315.
Welker, W. I. (1990). The significance of foliation and fissuration of cerebellar cortex. The cerebellar folium as a fundamental unit of sensorimotor integration. *Arch. Ital. Biol.* **128**, 87-109.
Wurst, W., Auerbach, A. B. and Joyner, A. L. (1994). Multiple developmental defects in Engrailed-1 mutant mice: an early mid-hindbrain deletion and patterning defects in forelimbs and sternum. *Development* **120**, 2065-2075.
Zong, H., Espinosa, J. S., Su, H. H., Muzumdar, M. D. and Luo, L. (2005). Mosaic analysis with double markers in mice. *Cell* **121**, 479-492.